EDGE ARTICLE

Check for updates

All publication charges for this article have been paid for by the Royal Society of Chemistry

Ratiometric fluorescent probes for capturing endogenous hypochlorous acid in the lungs of mice†

Xinfu Zhang, [iD] ‡[ab] Weiyu Zhao,‡[a] Bin Li, [iD] [a] Wenqing Li,[a] Chengxiang Zhang,[a] Xucheng Hou,[a] Justin Jiang[a] and Yizhou Dong [iD] *[acdefg]

Hypochlorous acid (HClO) is a promising diagnostic marker for inflammation and relevant diseases. Although many probes were previously developed for HClO imaging, the development of organ targeting probes is still lacking. Herein, we designed and synthesized a series of cyanine derivatives as ratiometric fluorescent probes to detect endogenous HClO in the lungs with inflammation. By installing diverse lipid chains and amino groups on cyanine, we identified that **ClO1**, with one *n*-octadecane chain and two 2-[[2-(dimethylamino)ethyl]methylamino]-ethyl groups, is a superior probe to target the lungs over other major organs in mice. **ClO1** was able to sense both exogenous and endogenous HClO in A549 (human lung epithelial) cells through fluorescence ratiometric imaging. In a lipopolysaccharide (LPS)-induced lung inflammation mouse model, **ClO1** effectively captured endogenous HClO in the lungs after intravenous administration. Overall, these cyanine-derived probes merit further development as organ targeting HClO sensors.

Introduction

Reactive oxygen species (ROS) and reactive nitrogen species (RNS) play critical roles in biological pathways and stress responses.[1–10] Hypochlorous acid (HClO), as one of the ROS molecules, is involved in multiple processes of the immune system, such as counteracting pathogens, suppressing inflammation and regulating cellular apoptosis.[11–14] Evidence has shown that an increased level of HClO is often found to be associated with human disorders, including inflammatory diseases.[15] Due to the important functions of HClO, previous studies have investigated a wide variety of fluorescent probes for detecting HClO. For example, probes established based on naphthalimides, acedan, cyanine dyes and other types of fluorophores were used to image HClO in living cells (Table S1†).[5,6,15–34] Many of these probes exhibited favorable features such as two-photon excitability or organelle targetability.[6,15,16,18,21,22,25,27,29–31,35] Among these previously reported HClO probes, a number of them were fabricated with cyanine dyes due to their high reactivity towards HClO.[17,23,36–38] A mechanism of reaction was previously proposed as shown in Scheme 1A.[23] In the presence of HClO, heptamethine cyanine dye (Cy7) undergoes an addition reaction to produce an intermediate. This intermediate then loses a HCl molecule and affords a Cy7 oxirane derivative, which exhibits shorter absorption and emission wavelengths compared to the original Cy7 molecule (Scheme 1A). This structural change enables Cy7 derivatives to be suitable ratiometric probes for HClO. The probes mentioned above are mainly applied in cell studies; however, it is urgent to develop probes for sensing HClO at the organ level for the potential diagnosis of diverse diseases. Previously, phenothiazine was modified with functional groups and a probe termed PMN-TPP was produced. This probe enabled the ratiometric fluorescence imaging of HClO in mice with skin inflammation.[6] Most recently, a probe derived from 2-methyl-1*H*-benzo[*de*]isoquinoline-1,3(2*H*)-dione was conjugated onto a diblock copolymer forming polymer micelles, which were used to image liver injury in zebrafish.[5] Despite these significant advances of diverse probes in the *in vivo* imaging of HClO, it is still of great demand to develop new types of organ targeting probes.

[a]Division of Pharmaceutics & Pharmaceutical Chemistry, College of Pharmacy, The Ohio State University, Columbus, Ohio 43210, USA. E-mail: dong.525@osu.edu

[b]State Key Laboratory of Fine Chemicals, Dalian University of Technology, Dalian 116024, China

[c]Department of Biomedical Engineering, The Ohio State University, Columbus, Ohio 43210, USA

[d]The Center for Clinical and Translational Science, The Ohio State University, Columbus, Ohio 43210, USA

[e]The Comprehensive Cancer Center, The Ohio State University, Columbus, Ohio 43210, USA

[f]Dorothy M. Davis Heart & Lung Research Institute, The Ohio State University, Columbus, OH 43210, USA

[g]Department of Radiation Oncology, The Ohio State University, Columbus, OH 43210, USA

Scheme 1   (A) Mechanism of heptamethine Cy7 for the ratiometric fluorescence imaging of HClO.[23] (B) Structures of probes **ClO1–ClO6**.

Results and discussion

In this study, we aim to design lung-targeting probes and detect HClO molecules in the event of inflammation. To date, numerous studies have explored lipid and polymer based nanoparticles for the delivery of therapeutic cargo to the lungs.[39–42] For example, researchers employed cationic or ionizable lipids to deliver DNA or siRNA to the lungs of mice.[40,42] Based on these studies, we speculate that lipid chains and amino groups may contribute to the accumulation of delivery materials along with their cargo in the lungs. Therefore, we conceived a series of heptamethine Cy7 based cyanine derivatives, **ClO1–ClO6**, as fluorescent ratiometric HClO probes (Scheme 1B). According to the methods reported previously,[23] **ClO1–ClO6** were synthesized through two-step reactions. The synthetic routes to **ClO1–ClO6** are described in the ESI.† The structures of **ClO1–ClO6** were confirmed by ^{1}H NMR and high-resolution mass spectrometry (ESI†). To confirm the mechanism shown in Scheme 1, we treated **ClO1** with HClO and measured the resulting product through mass spectra. A new

peak of m/z +16 was found (ESI, Fig. S1†), which corresponds to the epoxides produced by the oxidation of the double bonds in **ClO1** (Scheme 1A). This result is in accordance with the reported mechanism for the response of cyanine dyes towards HClO.[23] In order to study the effects of different functional groups, we installed long (n-octadecyl alkane, $C_{18}H_{37}$) and short (n-butyl, C_4H_9) lipid chains. Meanwhile, we incorporated diverse amino groups including 2[[2-(dimethylamino)ethyl]methylamino]-ethyl groups (**ClO1**), 3-(dimethylamino)-propyl groups (**ClO2** and **ClO6**), propyl-trimethylammonium groups (**ClO3**), and hexahydro-1H-azepine-1-ethanyl (**ClO4**). **ClO5** was synthesized as a control compound without amino groups.

In order to study the sensing ability of **ClO1–ClO6** towards HClO, we first performed a spectral study in solution with serial concentrations of HClO. Briefly, we investigated the absorption and emission spectra of **ClO1–ClO6** in phosphate buffered saline (PBS) by using a NaClO solution as the HClO source. Upon titration with NaClO, **ClO1** displayed a significant decrease in the absorption peak at 638 nm and a gradual increase in the absorption peak at 540 nm (Fig. S2†).

Meanwhile, we observed an evident decrease in the peak at 760 nm and an increase in the peak at 605 nm in the emission spectrum of **ClO1** with increasing concentration of NaClO (Fig. 1A, excited at 530 nm). Consequently, **ClO1** exhibited a dramatic fluorescence ratio (I_{605}/I_{760}) enhancement from 0.1 to 6.9 in a NaClO concentration range of 0–14 µM (Fig. 1B). The detection limit of **ClO1** was calculated to be 0.1 µM (Fig. S3†). In order to investigate the effects of different reactive oxygen species (ROS) and reactive nitrogen species (RNS) on **ClO1**, we performed a selectivity study. As shown in Fig. S4 and S5,† **ClO1** demonstrated a minimal absorption change at 638 nm and a minimal fluorescence change at 760 nm upon the addition of a wide variety of ROS/RNS, metal ions and amino acids, while an apparent decrease was seen after the addition of HClO. Therefore, the reactivity of **ClO1** towards HClO is much higher than that towards other ROS and RNS. Also, **ClO1** displayed a significant decrease in absorption at 638 nm and a decrease in fluorescence at 760 nm upon the addition of NaClO in the presence of Fe^{2+} and H_2O_2, but showed low reactivity with reduced glutathione (GSH) (Fig. S4 and S5†). Yet, local concentrations of these analytes may be different in both cells and tissues. In addition, we found that **ClO2**, **ClO4** and **ClO6** showed similar patterns of changes towards NaClO in both the absorption and emission spectra (Fig. S6, S8 and S10†). However, **ClO3** and **ClO5** exhibited strong fluorescence peaks at both 560 nm and 750 nm without the presence of NaClO, which makes them unsuitable for ratiometric fluorescence imaging (Fig. S7 and S9†). Therefore, **ClO1**, **ClO2**, **ClO4** and **ClO6** were selected for cell imaging studies.

Next, we applied **ClO1**, **ClO2**, **ClO4** and **ClO6** to detect exogenous HClO (NaClO solution) in live A549 cells (a human lung adenocarcinoma cell line). We found that these probes were able to stain A549 cells (Fig. 2 and S11–S13†). Consistent with the spectral study in solution, **ClO1** showed weak
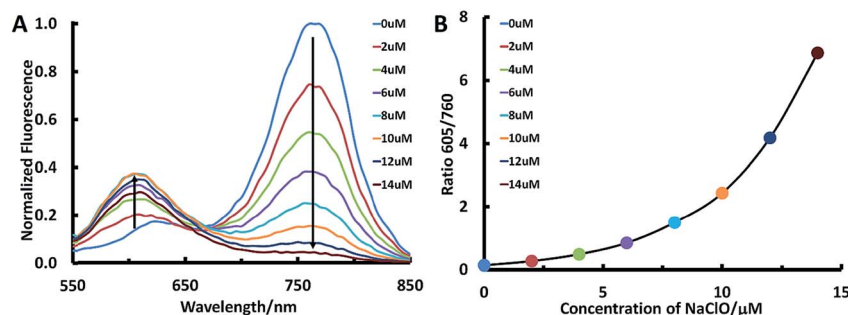

Fig. 1 (A) Emission spectra of **ClO1** (5 µM) upon treatment with various concentrations of NaClO (0–14 µM); (B) fluorescence ratio (I_{605}/I_{760}) of **ClO1** (5 µM) upon treatment with various concentrations of NaClO (0–14 µM).
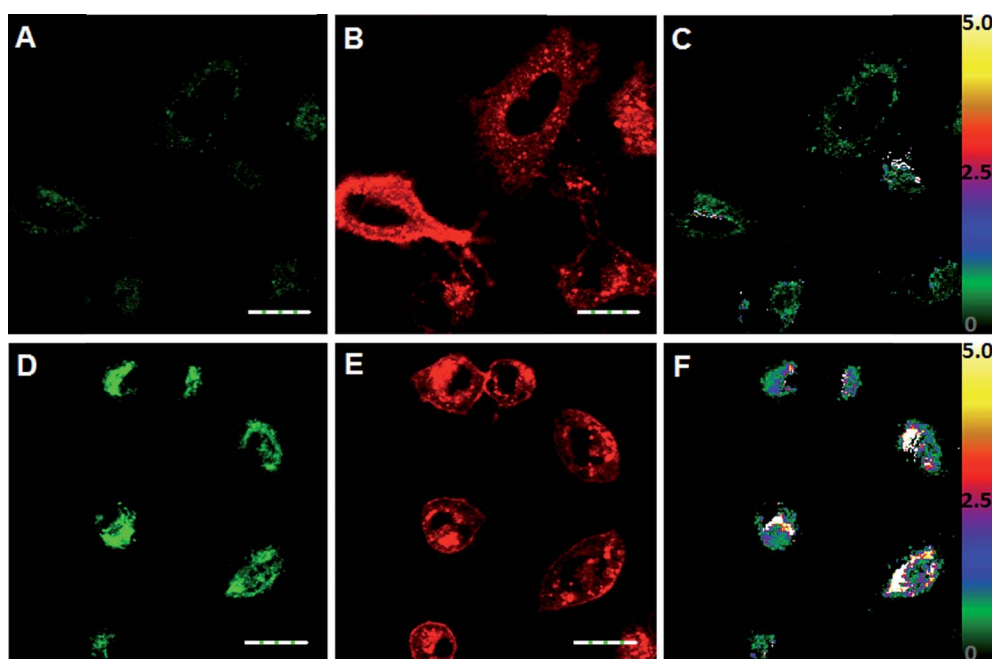

Fig. 2 Detection of exogenous HClO in A549 cells by **ClO1**. Cells were imaged with **ClO1** in the absence (A–C) or presence (D–F) of NaClO. (A) and (D) are green channels (560–660 nm); (B) and (E) are red channels (655–755 nm); (C) and (F) are the ratio images of the green/red channel. Scale bar = 20 µm.

fluorescence in the green channel (Fig. 2A, pseudo color green) and intense fluorescence in the red channel (Fig. 2B, pseudo color red) from the normal cell imaging. After treatment with NaClO, the cells displayed a remarkable enhancement in the fluorescence of the green channel (Fig. 2D) and a slight decrease in the fluorescence of the red channel (Fig. 2E). The ratio of the intensity in the two channels (green/red channel) increased dramatically from the baseline (Fig. 2C) to up to 5.0 (Fig. 2F), which indicates that **ClO1** possesses a robust ratiometric imaging property. **ClO6** displayed similar responses towards HClO in A549 cells to **ClO1** (Fig. S13†). **ClO2** and **ClO4** exhibited a much lower fluorescence enhancement in the green channel than **ClO1** and **ClO6** (Fig. S11 and S12†). Due to the high ratio enhancement in both the spectral study (0 to 6.9) and cell imaging (0 to 5.0), we selected **ClO1** for further *in vitro* and *in vivo* experiments.

In order to evaluate the ability of **ClO1** to detect *in situ* HClO production, we used lipopolysaccharides (LPS, endotoxins that cause the release of HClO in cells and animals[43]) to induce endogenous HClO production in A549 cells. Briefly, cells were further incubated with or without LPS for 24 h after staining with **ClO1**. We observed an apparent fluorescence increase in the green channel of cells treated with LPS (Fig. 3D) as compared to the control group without the treatment with LPS (Fig. 3A). An enhancement of the fluorescence ratio (green/red channel) was detected from 0 (Fig. 3C) to 2.5 (Fig. 3F) upon treatment with LPS. These results indicated that **ClO1** was able to capture HClO molecules generated from LPS treated cells. Furthermore, in order to study the cytotoxicity of **ClO1**, an MTT assay was performed using a series of concentrations of **ClO1**.

As shown in Fig. S14,† the survival rate was higher than 90%, suggesting low cytotoxicity of **ClO1** at the tested concentrations (0.5–10 μM).

Following the *in vitro* studies, we performed a biodistribution study of **ClO1–ClO6** in C57BL/6 mice. Indocyanine green (**ICG**, an FDA approved cyanine for fluorescence imaging in the clinic[44]) was used as a control. **ClO1–ClO6** and **ICG** were injected intravenously into mice. 1 h post injection, major organs (liver, lungs, spleen, kidneys, and heart) were harvested and imaged by using the IVIS fluorescence imaging system. **ClO1–ClO3** exhibited higher accumulation in the lungs than in other organs. **ClO4** and **ClO5** displayed higher distribution in both the spleen and lungs. **ClO6** and **ICG** showed a higher signal in the liver (Fig. 4). Based on the structural
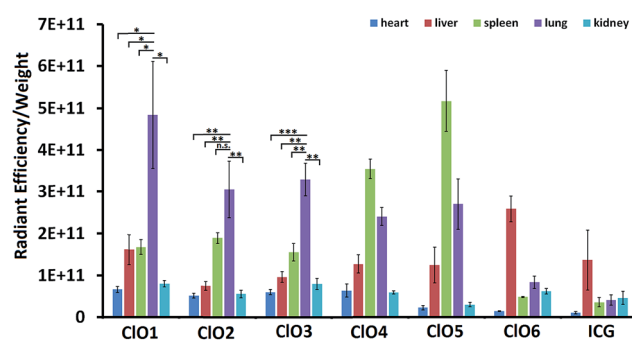
Fig. 4 The ratio of radiant efficiency to the organ weight of mice intravenously injected with **ClO1–ClO6** and **ICG**. ($n = 3$; *$P < 0.05$; **$P < 0.01$; ***$P < 0.001$; n.s., $P > 0.05$; t test, double-tailed).
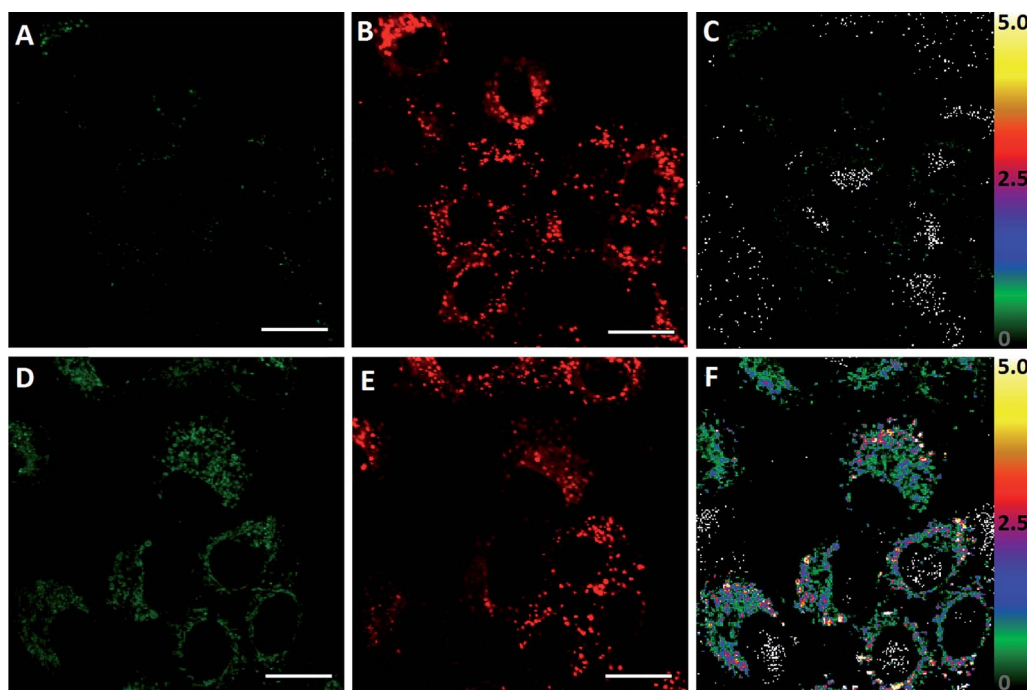
Fig. 3 Detection of endogenous HClO in A549 cells by **ClO1**. Cells were imaged with **ClO1** in the absence (A–C) or presence (D–F) of LPS. (A) and (D) are green channels (560–660 nm); (B) and (E) are red channels (655–755 nm); (C) and (F) are the ratio images of the green/red channel. Scale bar = 20 μm.
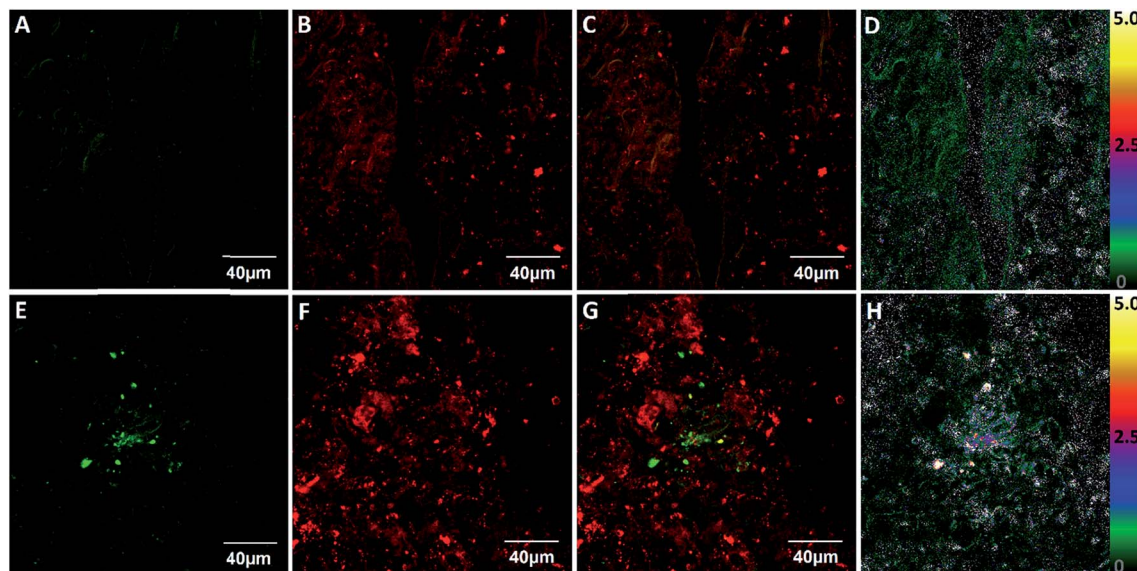
Fig. 5 Fluorescence imaging of the lung histology slides from mice intravenously injected with **ClO1**. (A–D) control mouse with intravenous injection of **ClO1**; (E–H) mouse treated with intranasal administration of LPS and intravenous injection of **ClO1**. (A) and (E) are green channels (560–660 nm); (B) and (F) are red channels (655–755 nm); (C) and (G) are overlay images of green and red channels; (D) and (H) are ratio images of green/red channels.

features of **ClO1–ClO6** and their corresponding organ distribution, we found that a long lipid chain was favorable for lung accumulation. Also, amino groups were a critical factor for lung targeting (**ClO1** *vs.* **ClO4**), and might be protonated in cells and produce positive charges. These results are consistent with previous reports that positive charges on nanoparticles affect their lung-targeting ability.[40,42]

Lastly, we studied whether **ClO1** was able to detect endogenous HClO at LPS-induced lung inflammation sites in mice. We first treated mice with LPS (intranasal administration) to induce acute lung inflammation. Then, we intravenously injected **ClO1** into both untreated and LPS-treated mice. 1 h after the injection, the lungs of the mice were dissected and sectioned into ~100 μm slices and imaged under a confocal microscope. Strong fluorescence was observed in the red channel of both slices, which confirmed the accumulation of **ClO1** in the lungs (Fig. 5B and F). Consistent with the *in vitro* results, many spots in the lungs treated with LPS produced a strong signal in the green channel (Fig. 5E), while minimal fluorescence was found in the green channel of the untreated lungs (Fig. 5A). The fluorescence ratio (green/red channel) at the inflammation sites was around 5.0 (Fig. 5H), which is much higher than that in the control lungs without inflammation (Fig. 5D).

Conclusions

In summary, we designed and synthesized a series of Cy7 based fluorescence ratiometric probes in order to detect HClO in the lungs. **ClO1–ClO3** with long hydrophobic lipid chains and hydrophilic amino groups showed high accumulation in mouse lungs after intravenous injections. However, **ClO4** with hexahydro-1*H*-azepine-1-ethanyl amino groups and **ClO5** with *n*-

butyl (without amino groups) showed a higher uptake in the spleen than in other organs tested. **ClO6** with short lipid chains displayed high distribution in the liver similar to **ICG**. These results indicated that both lipid chains and amino groups are important moieties for enabling the lung targeting effect of the probes. Moreover, an appropriate combination may dramatically increase the targeting specificity. Among these probes, **ClO1**, containing one *n*-octadecane chain and two 2-[[2-(dimethylamino)ethyl]methylamino]-ethyl groups, exhibited a sensitive fluorescence ratio response towards both exogenous and endogenous HClO in live cells. Based on the *in vivo* results, we demonstrated that **ClO1** was able to capture LPS-induced HClO in the mouse lungs. These findings can be applied to design new probes for non-invasive and real-time monitoring of HClO *in vivo* in the future.

Conflicts of interest

There are no conflicts to declare.

Acknowledgements

References

1 B. D'Autreaux and M. B. Toledano, *Nat. Rev. Mol. Cell Biol.*, 2007, **8**, 813–824.

2 T. Finkel and N. J. Holbrook, *Nature*, 2000, **408**, 239–247.

3 M. Valko, D. Leibfritz, J. Moncol, M. T. Cronin, M. Mazur and J. Telser, *Int. J. Biochem. Cell Biol.*, 2007, **39**, 44–84.

4 C. C. Winterbourn, *Nat. Chem. Biol.*, 2008, **4**, 278–286.

5 P. Zhang, H. Wang, Y. Hong, M. Yu, R. Zeng, Y. Long and J. Chen, *Biosens. Bioelectron.*, 2018, **99**, 318–324.

6 H. Xiao, J. Li, J. Zhao, G. Yin, Y. Quan, J. Wang and R. Wang, *J. Mater. Chem. B*, 2015, **3**, 1633–1638.

7 P. Zhang, Y. Tian, H. Liu, J. Ren, H. Wang, R. Zeng, Y. Long and J. Chen, *Chem. Commun.*, 2018, **54**, 7231–7234.

8 P. Zhang, X. F. Jiang, X. Nie, Y. Huang, F. Zeng, X. Xia and S. Wu, *Biomaterials*, 2016, **80**, 46–56.

9 P. Zhang, X. Nie, M. Gao, F. Zeng, A. Qin, S. Wu and B. Z. Tang, *Mater. Chem. Front.*, 2017, **1**, 838–845.

10 Y. Huang, P. Zhang, M. Gao, F. Zeng, A. Qin, S. Wu and B. Z. Tang, *Chem. Commun.*, 2016, **52**, 7288–7291.

11 C.-H. Sam and H.-K. Lu, *Journal of Dental Sciences*, 2009, **4**, 45–54.

12 C. C. Winterbourn, M. B. Hampton, J. H. Livesey and A. J. Kettle, *J. Biol. Chem.*, 2006, **281**, 39860–39869.

13 B. Kwaśny-Krochin, M. Bobek, E. Kontny, P. Gluszko, R. Biedroń, B. M. Chain, W. Maśliński and J. Marcinkiewicz, *Amino Acids*, 2002, **23**, 419–426.

14 M. Casciaro, E. Di Salvo, E. Pace, E. Ventura-Spagnolo, M. Navarra and S. Gangemi, *Immun. Ageing*, 2017, **14**, 21.

15 Y. W. Jun, S. Sarkar, S. Singha, Y. J. Reo, H. R. Kim, J.-J. Kim, Y.-T. Chang and K. H. Ahn, *Chem. Commun.*, 2017, **53**, 10800–10803.

16 L. Yuan, L. Wang, B. K. Agrawalla, S.-J. Park, H. Zhu, B. Sivaraman, J. Peng, Q.-H. Xu and Y.-T. Chang, *J. Am. Chem. Soc.*, 2015, **137**, 5930–5938.

17 H. Li, L. Guan, X. Zhang, H. Yu, D. Huang, M. Sun and S. Wang, *Talanta*, 2016, **161**, 592–598.

18 S.-k. Yao and Y. Qian, *Sens. Actuators, B*, 2017, **252**, 877–885.

19 L.-L. Xi, X.-F. Guo, C.-L. Wang, W.-L. Wu, M.-F. Huang, J.-Y. Miao and B.-X. Zhao, *Sens. Actuators, B*, 2018, **255**, 666–671.

20 Y. L. Pak, S. J. Park, D. Wu, B. Cheon, H. M. Kim, J. Bouffard and J. Yoon, *Angew. Chem., Int. Ed.*, 2018, **57**, 1567–1571.

21 P. Zhang, H. Wang, D. Zhang, X. Zeng, R. Zeng, L. Xiao, H. Tao, Y. Long, P. Yi and J. Chen, *Sens. Actuators, B*, 2018, **255**, 2223–2231.

22 B. Zhang, X. Yang, R. Zhang, Y. Liu, X. Ren, M. Xian, Y. Ye and Y. Zhao, *Anal. Chem.*, 2017, **89**, 10384–10390.

23 Z. Lou, P. Li, P. Song and K. Han, *Analyst*, 2013, **138**, 6291–6295.

24 L. Wu, I. C. Wu, C. C. DuFort, M. A. Carlson, X. Wu, L. Chen, C.-T. Kuo, Y. Qin, J. Yu, S. R. Hingorani and D. T. Chiu, *J. Am. Chem. Soc.*, 2017, **139**, 6911–6918.

25 M. Ren, B. Deng, K. Zhou, X. Kong, J.-Y. Wang, G. Xu and W. Lin, *J. Mater. Chem. B*, 2016, **4**, 4739–4745.

26 H. Zhu, J. Fan, J. Wang, H. Mu and X. Peng, *J. Am. Chem. Soc.*, 2014, **136**, 12820–12823.

27 L. Cao, R. Zhang, W. Zhang, Z. Du, C. Liu, Z. Ye, B. Song and J. Yuan, *Biomaterials*, 2015, **68**, 21–31.

28 J. Fan, H. Mu, H. Zhu, J. Wang and X. Peng, *Analyst*, 2015, **140**, 4594–4598.

29 Z. Qu, J. Ding, M. Zhao and P. Li, *J. Photochem. Photobiol., A*, 2015, **299**, 1–8.

30 C. Liu, X. Jiao, S. He, L. Zhao and X. Zeng, *Talanta*, 2017, **174**, 234–242.

31 K. Li, J.-T. Hou, J. Yang and X.-Q. Yu, *Chem. Commun.*, 2017, **53**, 5539–5541.

32 B. Zhu, L. Wu, M. Zhang, Y. Wang, C. Liu, Z. Wang, Q. Duan and P. Jia, *Biosens. Bioelectron.*, 2018, **107**, 218–223.

33 B. Zhu, L. Wu, M. Zhang, Y. Wang, Z. Zhao, Z. Wang, Q. Duan, P. Jia and C. Liu, *Sens. Actuators, B*, 2018, **263**, 103–108.

34 Y. Wang, L. Wu, C. Liu, B. Guo, B. Zhu, Z. Wang, Q. Duan, Z. Ma and X. Zhang, *J. Mater. Chem. B*, 2017, **5**, 3377–3382.

35 Z. Mao, M. Ye, W. Hu, X. Ye, Y. Wang, H. Zhang, C. Li and Z. Liu, *Chem. Sci.*, 2018, **9**, 6035–6040.

36 J. Peng, A. Samanta, X. Zeng, S. Han, L. Wang, D. Su, D. T. B. Loong, N.-Y. Kang, S.-J. Park, A. H. All, W. Jiang, L. Yuan, X. Liu and Y.-T. Chang, *Angew. Chem., Int. Ed.*, 2017, **56**, 4165–4169.

37 X. Jia, Q. Chen, Y. Yang, Y. Tang, R. Wang, Y. Xu, W. Zhu and X. Qian, *J. Am. Chem. Soc.*, 2016, **138**, 10778–10781.

38 D. Oushiki, H. Kojima, T. Terai, M. Arita, K. Hanaoka, Y. Urano and T. Nagano, *J. Am. Chem. Soc.*, 2010, **132**, 2795–2801.

39 E. R. Lee, J. Marshall, C. S. Siegel, C. Jiang, N. S. Yew, M. R. Nichols, J. B. Nietupski, R. J. Ziegler, M. B. Lane, K. X. Wang, N. C. Wan, R. K. Scheule, D. J. Harris, A. E. Smith and S. H. Cheng, *Hum. Gene Ther.*, 1996, **7**, 1701–1717.

40 R. Stribling, E. Brunette, D. Liggitt, K. Gaensler and R. Debs, *Proc. Natl. Acad. Sci. U. S. A.*, 1992, **89**, 11277–11281.

41 S. Azarmi, W. H. Roa and R. Löbenberg, *Adv. Drug Delivery Rev.*, 2008, **60**, 863–875.

42 O. F. Khan, E. W. Zaia, S. Jhunjhunwala, W. Xue, W. Cai, D. S. Yun, C. M. Barnes, J. E. Dahlman, Y. Dong, J. M. Pelet, M. J. Webber, J. K. Tsosie, T. E. Jacks, R. Langer and D. G. Anderson, *Nano Lett.*, 2015, **15**, 3008–3016.

43 C.-Y. Chuang, T.-L. Chen, Y.-G. Cherng, Y.-T. Tai, T.-G. Chen and R.-M. Chen, *Arch. Toxicol.*, 2011, **85**, 209–218.

44 G. Liberale, P. Bourgeois, D. Larsimont, M. Moreau, V. Donckier and T. Ishizawa, *Eur. J. Surg. Oncol.*, 2017, **43**, 1656–1667.